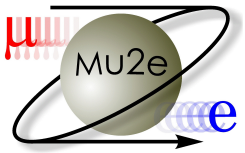

In situ monitoring of the stopped μ flux at Mu2e

Intern: Bastiano Vitali
Mu2e Fermilab - Summer Student Programme 2018
Dipartimento "E. Fermi", Università di Pisa

Supervisor: Pavel Murat
Co-Supervisor: Gianantonio Pezzullo

October 31, 2018

Abstract

The aim of this work is to be a guideline for future attempts to include two data-based strategies for the monitoring of the stopped muon flux at the Mu2e experiment. Here are exposed the motivations to make this inclusion and an early study. The approaches proposed here are to be intended as complementary to the already on study HPG detector. The proposed methods are counting of the DIOs and the protons ejected from the excited nuclei, after the muon capture. Both methods seem effective but sensitive to the flux variations on a different time scale. The rate of reconstructed DIOs is expected to be around 10 Hz, enough for a monitoring on the time scale of seconds. The efficiency reached for proton reconstruction as a function of momentum is presented and the number of reconstructed protons for each Event is ≈ 2.4, allowing sensitivity to variation on a scale of ms.

Contents

1 Introduction **2**
1.1 CLFV . . . 2
1.2 Mu2e apparatus . . . 2
1.3 Reconstruction . . . 3
1.4 Signal and background . . . 3
1.5 Monitoring of the μ flux . . . 3

2 Decay In Orbit **4**
2.1 DIOs pectrum . . . 4
2.2 DIOs frequency . . . 4

3 Protons **5**
3.1 Single proton event & efficiency . . . 5

4 Proton reconstruction in mix background **6**
4.1 Inefficiency of the tracker . . . 7
4.2 Future studies . . . 7

5 Conclusion **8**

Bibliography **8**

1 Introduction

1.1 CLFV

With the discovery and introduction of the neutrino oscillation, the extended SM predicts Charged Lepton Flavour Violation (Feynman diagram in Figure 1), with a BR too low to make possible a measurement (BR$< \mathcal{O}(10^{-52})$). Theories beyond the SM predict higher values for the BR, requiring direct measurements to discriminate among them.

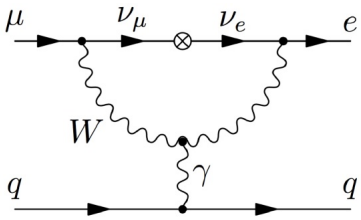

Figure 1: One of the Feynman diagrams of CLFV in the extended SM, precisely the muon-electron conversion in the nucleus field.

Various experiments searched for these processes and ended up setting upper limits for the BR, as shown in Figure 2. Regarding the $\mu \rightarrow e$ conversion, the last measurement was performed by SINDRUM II[2], which achieved Single Event Sensitivity[1] $\sim 10^{-13}$.

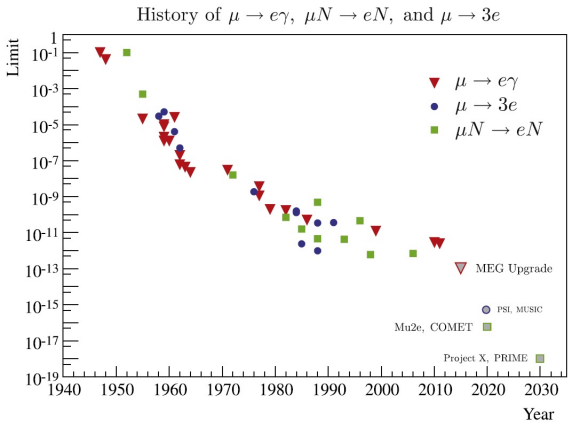

Figure 2: History of the CLFV searches [1].

1.2 Mu2e apparatus

The Mu2e experiment searches for CLFV looking at the conversion of μ in the nucleus field ($\mu^- + N \rightarrow e^- + N$) and the goal is a ses $\approx 3 \cdot 10^{-17}$:

$$R_{\mu e} = \frac{\Gamma(\mu^- + N \rightarrow e^- + N)}{\Gamma(\mu^- + N \rightarrow \text{All Captures})} < 3 \cdot 10^{-17} \text{ [3]}$$

A schematic of the apparatus is shown in Figure 3 and to get more information the Mu2e Technical Design Report [3] is the right place to start; here the experiment will be just summarized.

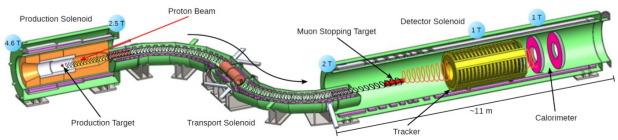

Figure 3: A schematic of the Mu2e experiment.

Every 1.4 s two proton bunches, containing $4 \cdot 10^{12}$ particles each and distant 43 ms, are extracted from the Fermilab Main Injector and enter in a accumulating ring. Trough resonant extraction, at the frequency of $\sim$ 600 kHz, portions of the bunches (*microbunches* of $3.9 \cdot 10^6$ protons) are directed on the production target. Thanks to the magnetic divergence and the position of the transport solenoid, only the particles produced backward are collected. This feature allows to reduce drastically the background and is one of the most prominent reason the goal ses is four order of magnitude lower then achieved by SINDRUM II. In the Production Solenoid and in the Transport Solenoid, the pions produced decay in muons. Thanks to the geometrical proprieties, only the μ^- arrive on the Stopping Target. The results of the interaction between these stopped muons and the nuclei are the particles the collaboration is interested in. Everything between two microbunches is called Event and its time structure is also shown in figure.

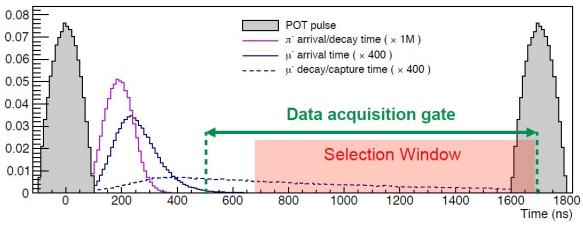

Figure 4: The time structure of an event.

In the Detector Solenoid there are two major components: the Tracker and the Calorimeter. The Tracker is made up by $\sim$ 23k straws filled with Ar:CO2. The straws are organized in twenty Stations, each made of two Planes. The single Plane

[1] The Single Event Sensitivity (ses) is the BR at which the experiment would see one event.

is formed by three trapezoidal Panels of two Layers of 48 straw tubes. As shown in Figure 5, the Panels are arranged in circle and the two Planes forming a Station are rotated to each other. The net effect achieved is an annulus straw-chamber whose radii define the momentum range of the detectable particles.
For our introductive purpose is sufficient to say that the calorimeter consists of two disks, as shown in figure 6. The sections are annular structures of ~ 674 CsI crystals, read by SiPMs.

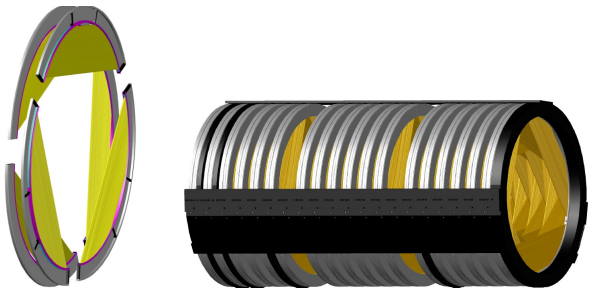

Figure 5: A schematic of the Mu2e tracker.

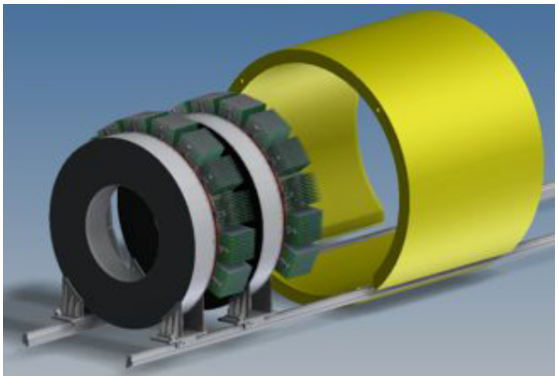

Figure 6: A schematic of the Mu2e Calorimeter.

1.3 Reconstruction

Given that center of this analysis is the reconstruction of the tracks in the Tracker, few words on how its done are needed.
The logic is fairly simple and illustrated here by steps:

- *StrawHit*: Particles ionize the gas in the straw tubes and the resulting charged showers generate an impulse on the wires
- *ComboHit* and *TimeCluster*: *SH* are grouped in space and time. The reason is to try to put the focus on the hits that may have been generated by the same particle.
- *HelixFinder*: A first 'fit' uses all triplets of *CH* to find circles in the x-y projection and use the distribution of the centers to find the center of the helix. It also estimate the step of the helix looking at the hits in the z-φ space.
- *TrackSeed*: A 3D fit performed using the helices found as initial values. No uncertainties are used in this procedure.
- *Track*: A Kalman filter[2] is used to improve accuracy in the reconstructed parameters of the *TrackSeed*, taking in to account: the drift time in the straw, the energy losses and the multiple scattering.

1.4 Signal and background

Looking for the $\mu \to e$ conversion, the signal of the experiment is a monoenergetic electron. The energy of this electron is given by the two body kinematics: $E_e = m_\mu - E_b(Z) - R_N(A) \approx 104.97$ [3] MeV, were $E_b(Z) \approx \frac{Z^2\alpha^2 m_\mu}{2}$ stands for the binding energy of the muon n the atom (aluminium is the element chosen for the stopping target [3]) and $R_N(A) \approx \frac{m_\mu u^2}{2m_N}$ for the recoil of the nucleus in order to conserve the momentum.
The muons arrive with flux ϕ_μ on the target and a fraction $f_{stop} = N_{stopped\ \mu}/N_\mu \approx 0.4$ is stopped, so the total flux of stopped muons is $\phi_{stop} = \phi_\mu f_{stop}$. Of these muons 39% decays while in orbit and 61% are captured by the nucleus. The background is then made up of:

- Electrons from the decays in orbit of the muons (DIOs) $\mu^- Al \to e^- \bar{\nu_e} \nu_\mu Al$
- Photons from radiative pion captures (RPC) $\pi^- Al \to \gamma Al^*$ and from radiative muon captures (RMC) $\mu^- Al \to \gamma \nu_\mu Mg$
- Protons ejected by the nuclear reactions following the muon capture
- Antiprotons produced in the production target by the 8 GeV proton
- Electrons and muons from the Cosmic Ray

1.5 Monitoring of the μ flux

Although being able to reconstruct and count the hypothetical conversions is of great importance, so it is to monitor, with the appropriate estimate of

[2]The basic functioning of a Kalman filter is quite straight forward: assuming the state in study can be described by a state vector, at each iteration the previous state and the new measurement are gauged trough a 'gain' and are used to evaluate the new state.

the uncertainties, the flux of the muons. The reason is that to yield a statistical significance to the measurement, this will be used as normalization.

An hardware implementation for this purpose, using a High Purity Germanium detector, is under development. The HPG will be use to measure photons produced by the interaction in the stopping target. The possibilities are:

- photons ($\sim$ 350 [keV]): produced by the de-excitation of the muonic atoms
- photons ($\sim$ 1800 [keV]): produced by the de-excitation of the nuclei after the muon nuclear capture ($\mu^- Al \rightarrow \nu_\mu Mg^*$, $Mg^* \rightarrow \gamma Mg^*$)
- delayed photons ($\sim$ 840 [keV]): produced by the de-excitation of the Al ($\mu^- Al \rightarrow \nu_\mu Mg^*$, β-decay, $Al^* \rightarrow \gamma Al$)

The study on the HPG detector is ongoing at AlCap, there are promising results and, to be thorough, the HPG spectrum is reported in figure 7.

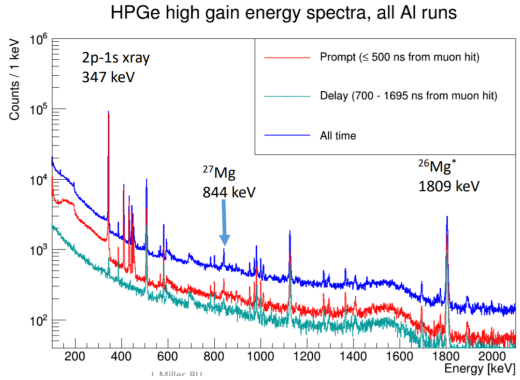

Figure 7: AlCap energy spectra of the HPG. [6]

Here we propose a parallel approach, exclusively data-driven. The idea is to use electrons from the decay in orbit of captured muons, which are easily reconstructed but probably too few, and protons ejected from delayed de-excitation of the nuclei after muons nuclear captures, which come in higher numbers but are more difficult to reconstruct. The first will be used to evaluate the absolute scale of the muon flux while the second to evaluate the relative fluctuations. In the next few pages will be explained why and how they can be used.

2 Decay In Orbit

The free muon decay ($\mu \rightarrow e\nu_e\nu_\mu$) produces an electron and two neutrinos. The end-point of the energy distribution of the electron (Michel spectrum) is at 52.8 MeV. When a μ^- is in $1S$ state and decays, the interaction with the nucleus modify the distribution of the electron energy, creating a long tail which reaches 105 MeV, the energy of the signal. Although high energy DIO are yet to be measured, they might be enough to be used as prompt for the flux monitoring.

2.1 DIOs pectrum

To predict the number of reconstructed DIOs, is necessary to evaluate their spectrum, the efficiency of electron reconstruction in the apparatus and convolve the two. The first distribution has already been studied [5][4] and is in Figure 8.

To estimate the reconstruction efficiency, 100k

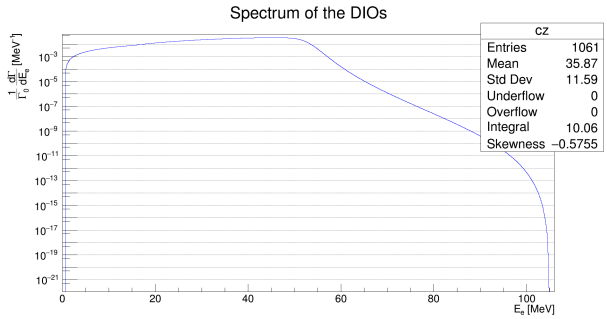

Figure 8: Spectrum for DIOs.

electron were generated with flat momentum distribution in the [60, 110] MeV range. The spectrum of the true momentum of the reconstructed electron was then divided for the production spectrum, obtaining the efficiency in Figure 9. The efficiency was then fitted with a Fermi-distribution-like function ($f = \frac{1}{1+exp(1+x)}$) and used to multiply the DIOs distribution. To be underlined is that the efficiency reaches $\sim$ 15% for high momenta electrons and decreases rapidly, going to 0 in the [70, 80] MeV region. For practical purpose we can consider the efficiency to be 0 below 80 MeV. The spectrum resulting from the convolution is shown in Figure 10 and doesn't decrease below 80 MeV due to the function chosen.

2.2 DIOs frequency

Given that only particles with roughly more than 80 MeV pass trough the tracker, to get the total number of particles the integration needs to be done from this values: $\int_{80}$DIOs dE[MeV] $\approx 1.98 \cdot 10^{-9}$. Knowing the rate of incoming protons ($3.6 \cdot 10^{20}/6 \cdot 10^7$ Hz), the fraction of μ stopped for proton ($2 \cdot 10^{-3}$) and the fraction of DIOs (≈ 0.39)

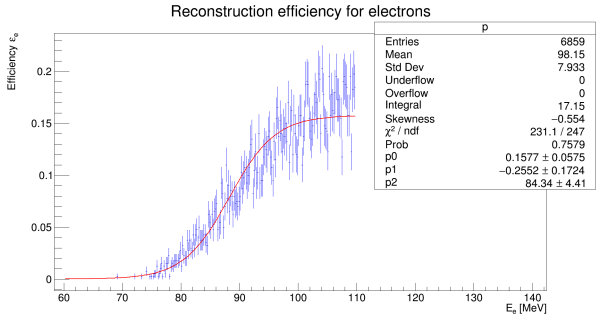

Figure 9: The efficiency for electrons: it reaches $\sim 15\%$ for $E > 100$ MeV and for practical purpose is negligible below 80 MeV.

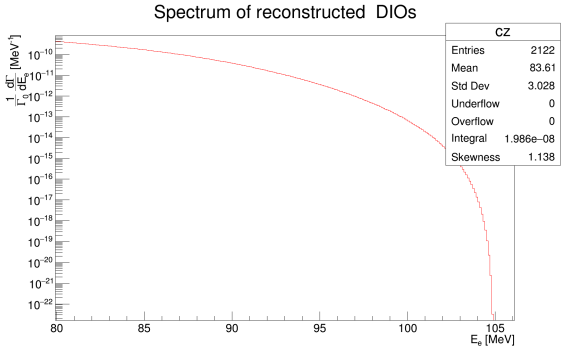

Figure 10: Endpoint of the spectrum of reconstructed DIOs.

is possible to evaluate the rate: $R_{DIOs} \approx 9.3$ Hz. The frequency of the reconstructed DIOs is then suitable for evaluate oscillation of ϕ only at a time scale of seconds.

3 Protons

While 39% of the stopped muons decay in orbit, 61% is captured by the nucleus with a consequent excitation. In $\sim 3\%$ of the cases, de-excitation can lead to a delayed proton emission by the nucleus. The expected rate is therefore ≈ 0.18 GHz.
Assuming that the fraction of ejected protons for stopped muons is constant in time, is possible to measure it over a long period, evaluating the number of muons, for example, with the DIOs counting. At this point to evaluate the fluctuations of the muons flux is possible to counting the protons over a shorter time period.
While in principle the concept is very easy, so is not the reconstruction. The reason is that the software has been optimized to the electron reconstruction. Proton trajectories are quite different, mostly because of the low $\beta \sim 0.1$ which translates in high energy deposit in the tracker (Bethe-Bloch trend $\sim 1/\beta^2$) and higher multiple scattering ($\sim 1/\beta p$).

3.1 Single proton event & efficiency

Reconstructing event of single proton was the first step, first with a well defined momentum, then with the expected spectrum for delayed emission proton, shown in Figure 12. Avoiding the confusion of multiple particles entering the tracker, has been possible to make the rough adjustment to adapt the fit routine to the protons tracks. An example of reconstructed proton from particle gun is in Figure 11.

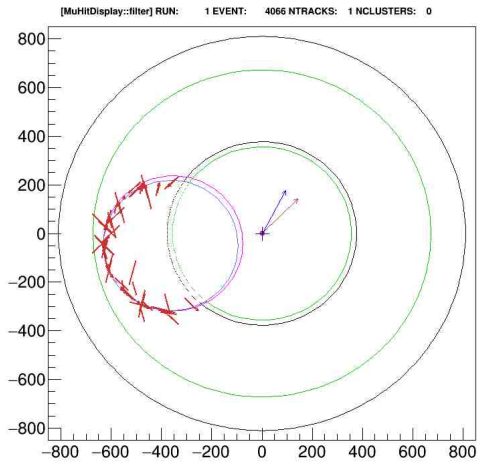

Figure 11: The first reconstructed proton in this analysis. The red lines are the uncertainties along the wires.

Some change were made on the file that configures the reconstruction. The key changes are here listed:

- Adjusting the search for the step of the *HelixFinder*
- The bit-flag used by the *Helixfinder* for tagging the δ-rays was turned off (protons' high charge hits are sometimes mistaken for δ's)
- Was increased the tmax for the *TimeClusterFinder*, from 1700 ns to 1800 ns (protons are slower then electrons and some of them reached the Tracker after after the time cut)

After this (rough) tuning, a sample of 10M protons was produced with the known spectrum (Figure 12), in order to evaluate the single proton reconstruction efficiency. Like for the DIOs, the efficiency was obtained dividing the spectrum of the true momentum of the reconstructed particles by the generated spectrum.

The obtained efficiency is in Figure 13. The maximum is around $\sim 10\%$ for protons of ~ 200 MeV and goes down quickly to low momenta. This is due to the high energy losses for slower particles. Meanwhile the trend for higher momenta has not yet been understood.

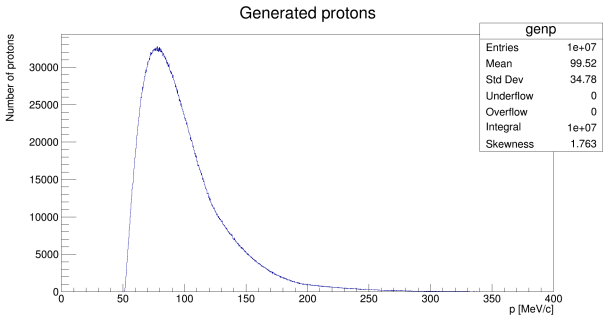

Figure 12: The 10M generated protons, following the spectrum for ejected protons from the nucleus.

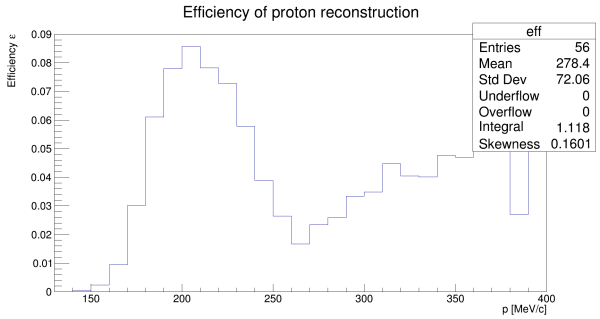

Figure 13: Efficiency of single proton reconstruction. The fast descending trend on the left is due to the energy losses, while the right rise is still to be understood.

As a check for the left side trend, a scatterplot of the reconstructed momentum vs the generated one was produced and is in Figure 14. Here is easy to see that for momenta lower than 250 MeV, the reconstructed momentum is systematically lower. The reason is probably that slower protons loose energy faster and the path from the stopping target to the tracker (which cross the proton absorber too) is no more negligible. Moreover, less energy means less SH, so slower protons are harder to reconstruct.

4 Proton reconstruction in mix background

The next step was to check if the fit was robust enough to reconstruct protons also in a mixed background data set. For this purpose

Figure 14: Reconstructed p vs generated. The lowering on the left side is due to the energy losses in the path from the stopping target to the tracker.

the NoPrimary-mix.MDC2018 dataset was used, in which each event is an whole 'Mu2e event', so everything produced by the incoming microbunch. Given that the backtracking of the track to the Montecarlo truth had some issue, probably due to the procedure of digitalization and compressing of the MC data, it has not be possible to evaluate the proton reconstruction efficiency in this case. In Figure 15 is shown an example of event. Here 3 proton tracks have been reconstructed.

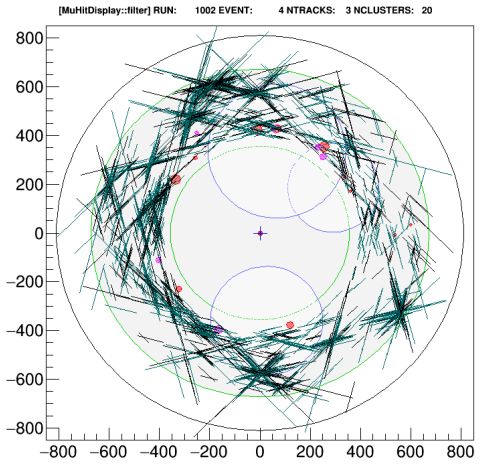

Figure 15: An example of event of the proton reconstruction runned on a NoPromary-mix.MDC2018 event. In this, three proton tracks were reconstructed.

The fundamental question is now at which timescale the proton counting is feasible. To answer, the number of reconstructed tracks per event was plotted and is reported in Figure 16. We can see that on average ≈ 2.4 protons are reconstructed per event. Remembering that the spacing between the two proton pulses is ~ 2 μs, the number of reconstructed protons should then be enough for a ms time scale variation monitoring.

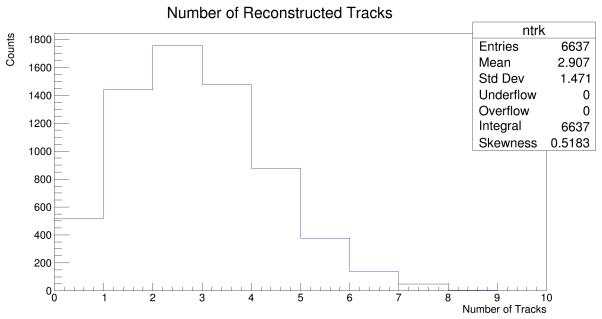

Figure 16: Number of reconstructed tracks per event, using the NoPrimary-mix.MDC2018a dataset. The mean is ≈ 2.4.

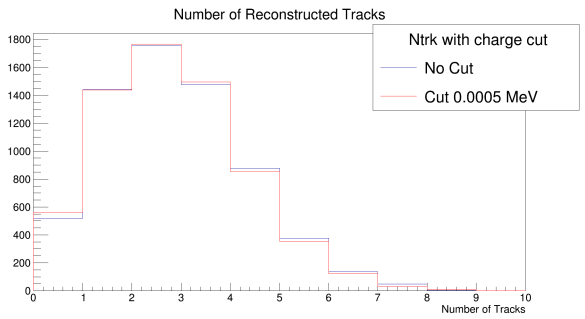

Figure 18: Comparison between number of reconstructed tracks per event with and without applying the cut on the straw hits energy.

4.1 Inefficiency of the tracker

The correlations of the number of reconstructed tracks with external factors are not trivial and need a in depth study, also in order to evaluate the systematic uncertainties related. One of the parameters which can be changed is the minimum energy required for an 'effective' straw hit. A cut on this parameter is a simple model for inefficiency in the single hit reconstruction and is important to understand if the distribution of the reconstructed tracks change drastically. The distribution of the SH energy, for the dataset used, is shown in Figure 17. Assuming that will be lost the straw hitswith lower energy, for example due to threshold, a cut at 5 keV was applied, also shown in Figure 17, and the tracks were reconstructed again. The histograms with and without the cut are shown in Figure 18. We can see that the distribution are quite similar, suggesting that the reconstruction is stable in respect to this parameter. The reason for this stability is the distribution of straw hits energy for each particles, shown in Figure 19. The straw hits from protons are generally more energetic, as already underlined, due to the low β. As a consequence, rising the cut on the straw hits charge should remove only straw hits from

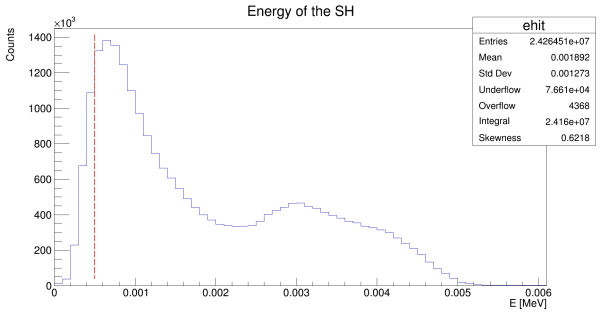

Figure 17: Distribution of the straw hits energy for the NoPrimary-mix.MDC2018a dataset.

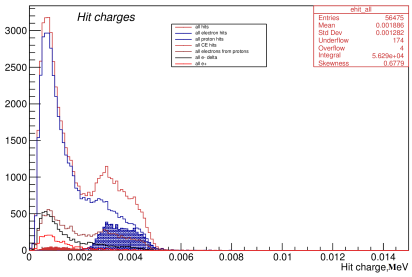

Figure 19: In the straw hits energy distribution is possible to appreciate the different contribution of different particles.

electrons, leaving the tracker reconstruction algorithm to deal with less hits in the tracker. Looking at Figure 19, the cut seems to be applicable up to around 0.002 MeV.

4.2 Future studies

Timing

Remembering that each event lasts for 1695 ns, the number of reconstructed protons per event translate to a nominative frequency of $\approx$ 1.4 MHz. If every event would be written on disk, on average, 100 μs would be enough to have a statistic uncertainty of $< 10\%$. The issues rise from the fact that this monitoring needs to be done online but the trigger will not accept every events and the reconstruction takes too long. As a consequences, could be important to speed up the proton reconstruction and evaluate the time budget needed.
In this direction, applying an higher cut on the straw hits charge would reduce the number of hits the reconstruction algorithm has to deal with, hopefully reducing the running time. Future study on this matter needs to be done. Another interesting question will be to understand if, in

the online monitoring, the whole fitting procedure is needed. Given that not many tracks are misleading when reconstructing protons, an appropriate study could find out if the Kalman filter can be skipped, resulting in a faster procedure.
Using the existing algorithm, no cuts and assuming only 1% of the events will be analyse, we aspect this method to be sensible to variations on the time-scale of ten milliseconds.

Dependence from the beam luminosity

Due to the absence of the number of proton per microbunch in the MDC2018a data sets, this part of the analysis has not been done. The question is how to evaluate the efficiency ε, assuming a generic dependence of the efficiency from the instantaneous luminosity of the beam and a generic distribution in time for the luminosity itself.
Probably a good solution would be to convolve the normalized distribution of the proton number per microbunches with the efficiency, as a function of the number of protons. The best estimate of ε would then be the mean of the obtained distribution and its standard deviation the systematic uncertainties.

5 Conclusion

The aim of this two months program was to find out if a data-driven stopped muon flux monitoring was possible, using DIO and proton reconstruction. As summarized in this brief report, after the evaluation of electron reconstruction efficiency, the rate of expected DIOs was found to be < 10 Hz. With this frequency, is possible to evaluate the flux and to be sensitive to variation on timescale of seconds. The reconstruction of protons needs to be optimize and the efficiency studied, in particular the effect for higher momenta. With this first rough tuning more then 2 protons are reconstructed per Event, allowing a sensitivity to variation on time scale of ms.
The cut on the straw hits seams a promising way to reduce the time needed for the reconstruction and a study on the effect on the efficiency is needed, as well as other studies on the robustness of the procedure.

References

[1] R. Bernstein and P. Cooper, *Charged lepton flavor violation: An experimenter's guide*, Physics Reports, 532 (2013), pp. 27–64.

[2] W. Bertl, *A search for $\mu-e$ conversion in muonic gold*, Eur. Phys. J., 47 (2006).

[3] M. Collaboration, *Mu2e technical design report*, tech. rep., Fermi National Accelerator Laboratory Batavia, IL 60510, October 2014.

[4] A. Czarnecki et al., *High-energy electrons from the muon decay in orbit: radiative corrections*, arXiv, (2015).

[5] A. Czarnecki and R. Szafron, *Muon decay in orbit: spectrum of high-energy electrons*, arXiv, (2011).

[6] J. Miller, *Stopping target monitor plans*, Mu2e-doc 18630-v1.